Preliminary Results of the THOR7 Propagation Experiment in the North Pole Region

Julien Queyrel, Xavier Boulanger, Laurent Castanet, James Nessel, Michael Zemba, Torgeir Prytz, Antonio Martellucci

Preliminary Results of the THOR7 Propagation Experiment in the North Pole Region

Julien Queyrel, ONERA/DEMR, Université de Toulouse, F-31055 Toulouse, France, +33 5 6225 2792, julien.queyrel@onera.fr
Xavier Boulanger, ONERA/DEMR, Université de Toulouse, F-31055 Toulouse, France, +33 5 6225 2880, xavier.boulanger@onera.fr
Laurent Castanet, ONERA/DEMR, Université de Toulouse, F-31055 Toulouse, France, +33 5 6225 2729, laurent.castanet@onera.fr
James Nessel, NASA Glenn Research Center, 21000 Brookpark Rd. MS 54-1, Cleveland, OH 44135, +1 216-433-2546, james.a.nessel@nasa.gov
Michael Zemba, NASA Glenn Research Center, 21000 Brookpark Rd. MS 54-1, Cleveland, OH 44135, +1 216-433-2546, michael.j.zemba@nasa.gov
Torgeir Prytz, Kongsberg Satellite Services, NO-9171 Longyearbyen, Norway, +47 79 02 25 64, torgeir@ksat.no
Antonio Martellucci, ESA/ESTEC, Keplerlaan 1 Noordwijk ZH, The Netherlands, +31 715655603, antonio.martellucci@esa.int

Abstract

A propagation experiment funded by ESA with support from CNES has been deployed in Svalbard (Northern Norway, 80° latitude North) in order to study propagation impairments at Ka-band caused by the troposphere at high latitudes and low elevation angles in representative conditions for GEO satcoms systems in the Artic region. In this context, a NASA Glenn Research Centre beacon receiver, operated by KSAT in Norway, measures the signal from the THOR7 satellite at a 2.65° elevation angle since March 2016. ONERA processes and analyses the data since the beginning of the experiment. At this stage 2 years of propagation data from the satellite have been gathered. An Atmospheric Numerical Simulator relying on the high resolution meteorological model (WRF-ARW) is used to generate 3D states of the atmosphere during a concurrent period to the experiment at high spatial & temporal resolutions. Propagation calculations based upon those outputs are then conducted to derive simulated attenuation time series between the beacon receiver and THOR7. Results show a fairly good statistical agreement between the measured and simulated attenuation time series whereas the simulated statistics seem to underestimate the overall attenuation for all percentages of time.

1 Introduction

The North Pole area is of increasing importance due to natural resources such as fishing industry and oil/gas exploration, and shipping routes are nowadays opening in those regions as a result of global warming. Together with them comes a growing need for communications at Ka-band and above, that could be fulfilled which GEO satellites or possible LEO satcom constellations (OneWeb, LEOSAT, Starlink). Those regions are also of great interest for increasing the amount of data transferred by Earth Observation data downlink systems because visibility periods of the satellite from the Earth station happen more often within a day for a polar orbit.

For decades, various Earth-space propagation experiments have been carried out above 10 GHz (SIRIO [1], ETS-II [2], ACTS [3], INTELSAT [4], COMSTAR [5], OLYMPUS [6], ITALSAT [7], ALPHASAT [8]) and allowed significant progress in the understanding and the modelling of the propagation channel at mid-latitudes. The communication link with a GSO satellite in the Artic region however suffers from specific propagation conditions that cannot be easily investigated at those latitudes: very low elevation (down to 5°) and specific impairments (large and small scale refraction, wet snow attenuation…) are not (or poorly) taken into account in conventional propagation models.

In order to investigate the Ka propagation channel in those regions, ESA funded a propagation experiment with the THOR-7 GEO satellite ($\varphi = 1°$W), from the NASA Glenn Research Centre beacon receiver (20.198 GHz) installed at the Svalbard Satellite teleport (SvalSat) operated by KSAT in the Sptizberg island of the Svalbard archipelago in Norway [ref]. With the help of NASA, ONERA is in

charge of the data analysis of the beacon signal level and surface meteorological parameters measurements. Extra funding from the French space agency (CNES) allows ONERA to investigate further the low elevation large scale refractive effects by conducting concurrent atmospheric simulation based on the high-resolution numerical meteorological model WRF-ARW. Extensive propagation calculations allow the generated 3D state of the atmosphere to be converted into total attenuation time series, as seen by the beacon receiver at Svalsat.
This paper describes the propagation experiment conducted with the THOR7 satellite at Svalsat, (section 2) and the methodology used to estimate the attenuation time series and statistics acquired for 2 years between April 2016 and March 2018 (section 3). Section 4 gives a detailed description of the meteorological numerical model used to generate the atmosphere and the computations allowing for the retrieval of the total attenuation. Finally, section 5 gathers the results of the comparison between the generated and measured attenuations series.

2 Ground station & data acquisition

The experiment ground station consists in a beacon receiver designed by the NASA Glenn Research Centre [9] that operates in the Ka-band at the 20.198 GHz beacon frequency of the THOR-7 satellite which is seen at a 2.65° elevation angle from SvalSat. A Ka-band radiometer (Radiometrics PR-2230) that can observe multiple channels between 22 and 30 GHz is also available on site. Other meteorological instruments such as an optical rain-gauge (Optical Scientific Instruments, ORG-815), a tipping bucket rain-gauge and a weather station equipped with an IR cloud sensor complement the equipment deployed for this experiment. The beacon signal (circular polarization) is reflected by a 1.2 meter Cassegrain antenna ($G = 45$ dBi), then both co- and cross-polar signals are amplified through a LNA ($G = 44$ dB, $NF = 1.4$ dB) and down-converted into the final intermediate frequency ($IF = 70$ MHz) to be digitalized and processed by a SDR FFT-software implementing a modified version of a Quinn-Fernandez frequency estimation [10].

3 Data processing

3.1 Noise power inversion

Due to the inherent difficulties of the propagation campaign architecture in Svalbard (extremely low elevation angle of 2.65°) and issues with accumulated wet snow on the radiometer that induce a wrong inversion of radiometric data, a novel approach [11] for measuring the sky brightness temperature along the line-of-sight path from the beacon receiver to the THOR 7 satellite was investigated during the experimental campaign. Using an adaptive notch filter to remove the signal from the power spectrum of the beacon receiver, the total noise power can be integrated to provide an estimate of the impact of the sky noise on the total system noise.

The following steps are preformed to calibrate the noise power and convert it into a sky brightness temperature: (i) first a 1-hour block timescale average of the 10 Hz noise power and beacon receiver time series is performed, (ii) days with stable clear sky attenuation are identified (rain gauge tipping bucket, minimal variation of signal), (iii) ECMWF ERA5 data are used over the entire month on those days to define a monthly mean clear sky attenuation and mean radiating temperature value, (iv) a clear sky level offset is calculated from the receiver power level for each month in order to calibrated coarsely the beacon-derived attenuation, (v) the RTE is used to convert beacon-derived attenuation to equivalent brightness temperature, (vi) scaling coefficients (a, b) are obtained by fitting linearly the 1-hour beacon-derived brightness temperature to the 1-hour noise power levels: $T_{sky} = a \times N_{pwr} + b$. Results of the procedure for two months are illustrated in Figure 1.

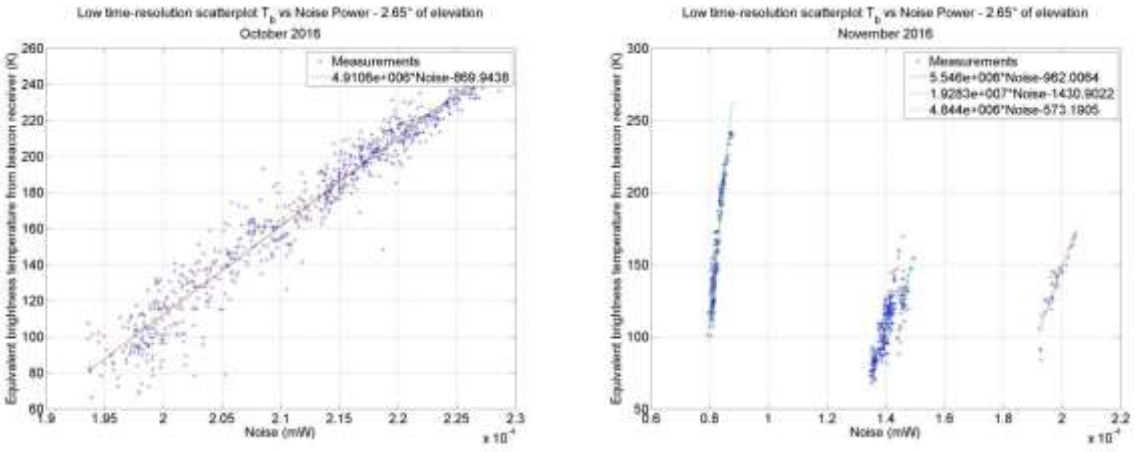

Figure 1 – Correlation between the T_{sky} measured from the beacon attenuation and the noise power integrated on the 1 MHz beacon reciever bandwidth for October & November 2016.

Comparisons are made between the direct line-of-sight noise power inversion approach and the scaled (10° to 2.65°) radiometric measurement and show good agreement in most cases.

3.2 Total attenuation time series

In order to derive the total attenuation time series, a visual inspection of the data is required on a daily basis. The inspection allows to spot spikes and invalid data acquisitions, but ultimately aims at identifying precipitation events (t_{start} and t_{end}) when scattering effects are not negligible anymore. Several sources of information are used for this identification: the beacon data itself, the tipping bucket and optical rain gauge measurements, the radiometric measurements associated with the noise power inversion results, and the integrated liquid water contents. Outside of those events the beacon data can be scaled to total attenuation using the absorbing attenuation derived from the noise power inversion, whereas inside those events a linear interpolation of the absorbing attenuation levels at t_{start} and t_{end} is performed.

3.3 Experimental results

From April 2016 to March 2018 valid in-excess (resp. total) attenuation measurements have been collected with an availability of 92.03% (resp. 91.98 %) of the time: 93.27% (93.17 %) the first year and 90.79% (90.79 %) the second year. Surface parameters, including tipping bucket rain gauge measurements are available for 91.71 % of the time (91.67 % the first year, 91.75 % the second year), and the data collected from an optical rain gauge are available for 71.76 % of the time (79.63 % the first year, 63.88 the second year). In Figure 2 examples of attenuation (in-excess and total) are shown for two distinct months.

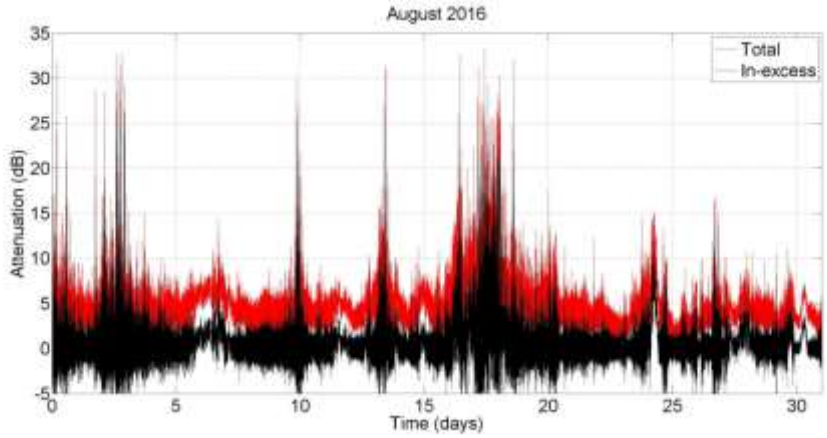

Figure 2 – In-excess and total attenuation time series measured by the THOR7 beacon receiver after data processing (August 2016 & January 2017)

Various CCDF of the rainfall rate are plotted in the left panel of Figure 3: the optical rain gauge CCDF is computed using the total rainfall (dotted curve), using only the data when $T_{surf} > 0$°C (cyan curve), or using only the data except when the condition code of the instrument is 'snow' (cyan dotted curve). The differences between the curves show the difficulty in estimating the actual rainfall rates: the presence of snow and the impact of freezing temperature on the instruments operations are supposed to be responsible for those behaviours.

Statistical analyses have also been conducted for the in-excess and total attenuation measured time series. After removing the scintillation using a raised cosine filter with a 0.01 Hz cut-off frequency [12], the CCDF plotted in the right panel of Figure 3 are derived. Monthly statistics of the attenuation have also been computed: they show an increase in attenuation exceeded for any percentages during the summer period.

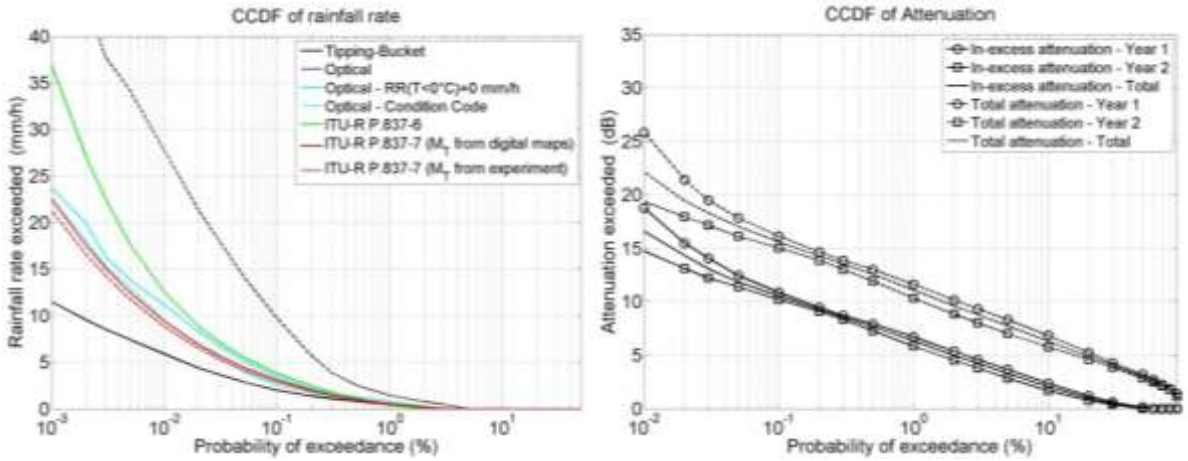

Figure 3 – Experimental CCDFs for rainfall rates (left) and in-excess and total attenuation (right) during the 2 years (April 2016 – March 2018) of the experiment

The scintillation has been extracted using the same raised cosine filter with 0.01 Hz cut-off frequency. Its standard deviation has been computed over 60 seconds' periods. Results for the 2 years are gathered in Figure 4.

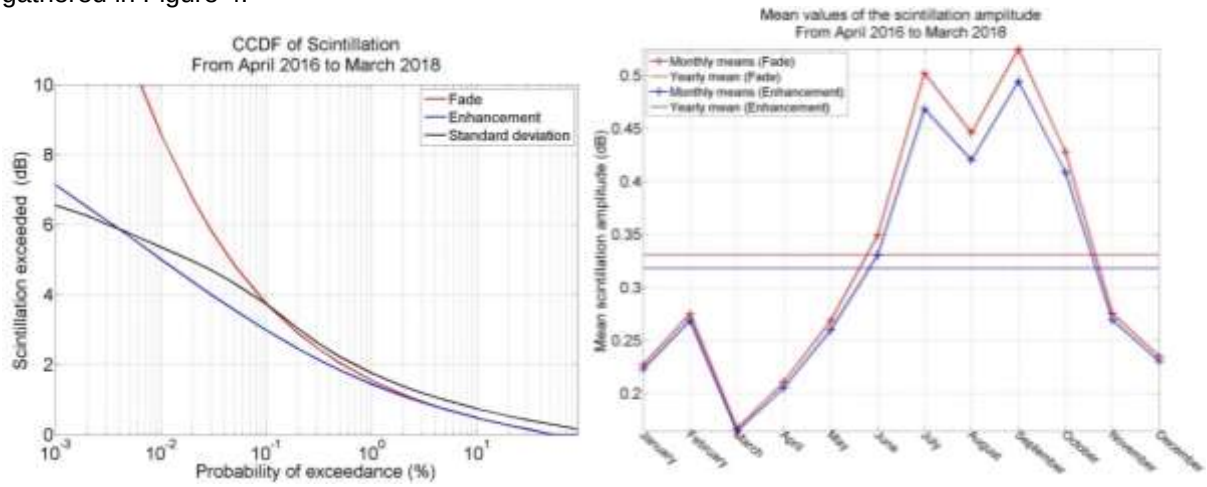

Figure 4 – CCDF of scintillation (fade, enhancement and standard deviation) (left) and monthly standard deviation (right)

4 Atmospheric Numerical Simulator (ANS)

4.1 Generation of the atmosphere

In order to compute the propagation conditions along the THOR7 link towards the beacon receiver, an atmospheric numerical simulator has been used along with an electromagnetic module [13], [14]. The high-resolution numerical weather prediction model WRF-ARW (v3.4) [15] is used to generate a 4D description of the atmosphere around the beacon receiver at a high temporal (5 min) and spatial resolution (2 km). The datacubes thus produced are approximately 160 km x 160 km horizontal squares and 36 vertical model levels span ~ 20 km of atmosphere. The meteorological model is initialized with the ECWMF ERA-Interim re-analysis database which provides surface and pressure levels parameters every 6 hours with a 0.75° resolution. These same re-analysis data are also used by WRF-ARW as boundary conditions every 6 hours. In order to mimic realistic passed states of the atmosphere, simulations are limited to one day with a previous 12 hours spin-up period (the results of which are deleted latter-on) giving the opportunity to the model to provide stable outputs. In order to reach the 2km resolution, 3 nested domains are used: a coarser domain with a 30 km resolution on a polar stereographic projection and static fields initialized directly by way of an interpolation from the ERA-Interim database, and two successive nests at 6 km and 2 km resolution (see Figure 5).

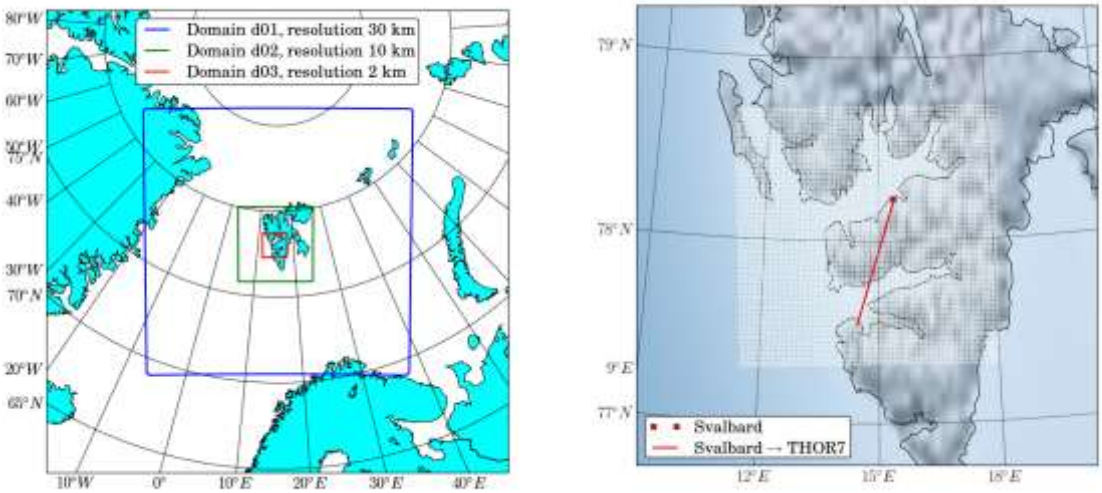

Figure 5 – The 3 nested geographical domains of the WRF-ARW simulation (left), and position of the high-resolution domains d03 with direction of the THOR7 satellite (right)

4.2 Attenuation retrieval

The atmospheric parameters of interest (P, T, $\rho_{vap}, \rho_{cloud}, \rho_{rain}$) are then converted by an electromagnetic module written in Python into specific attenuations (dB/km) of the various constituents of the troposphere known to produce attenuation effects at Ka-band frequencies: water vapour, oxygen, clouds and rain (see integrated columnar contents in Figure 6). At this point in the study, attenuation due to snow is not modelled by the electromagnetic module. The physical models used by the module are: the line-by-line spectral model of Recommendation ITU-R P.676-11 (annex 1, §1) for oxygen (γ_{ox}) and water vapour (γ_{vap}) and the model based on Rayleigh scattering of Rec. ITU-R P.840-7 (annex 1, §2) for clouds droplets ($\gamma_{cloud} = K_l(f,T) \times \rho_{cloud}$). Rain specific attenuation (γ_{rain}) is derived from Mie's theory (extinction cross-section $\sigma_{ext}(D)$) assuming spherical droplets and a Marshall-Palmer raindrop size distribution ($N(D) = N_0 e^{-\Lambda D}$) which slope parameter Λ is fixed by the precipitating water content of each pixel cube (ρ_{rain}) [16]:

$$\gamma_{rain} = 4.343 \times 10^3 \int_0^{D_{max}} \sigma_{ext}(D) N(D) dD$$

The Mie's coefficients used to infer $\sigma_{ext}(D)$ being computationally expensive to derive, a look-up table linking T and ρ_{rain} to γ_{rain} is used.

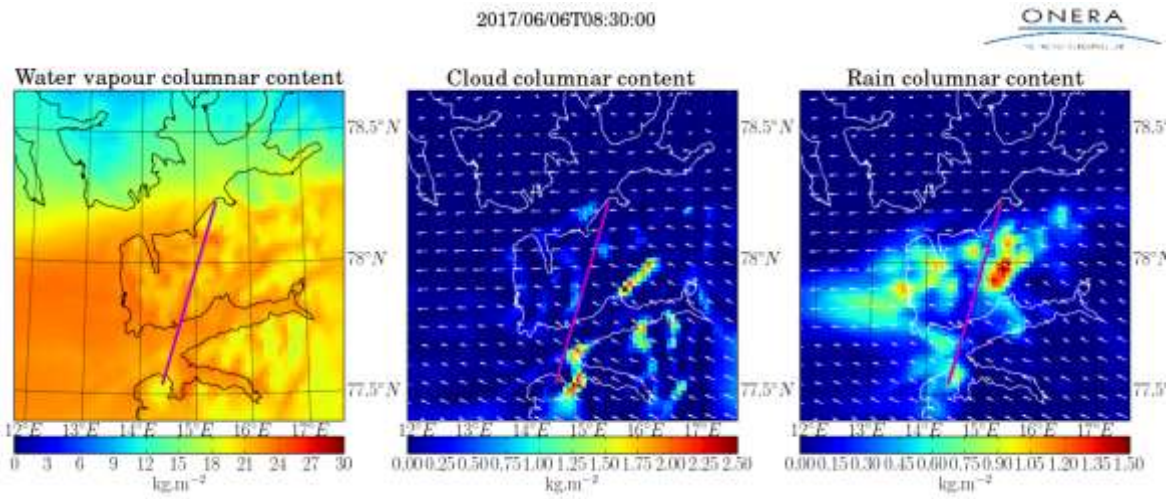

Figure 6 – Integrated water vapour (left), cloud (middle) and rain (right) content on the last domain centered around Svalsat at a specific time step of the simulation (2017/06/06T08:30)

In order to compute the total attenuation suffered by the signal when reaching the beacon receiver at low elevation angle ($\theta \sim 2.65°$) large scale geometric refractive effects are taken into account. First, for each time step a vertical slice of atmosphere, directed toward the satellite (azimuth ψ), is extracted from the WRF datacube (see Figure 7). Then, a dichotomy algorithm is used to estimate the actual elevation angle and geometric path between the beacon receiver and the satellite by propagating a geometric ray through the various layers of atmosphere within the slice. To that aim, the refractive index of all points within the slice are computed from P, T and ρ_{vap} (*cf.* Rec. ITU-R P.453-13) and Snell/Descartes' geometric laws are used as suggested in the spherically layered atmosphere model of ITU-R P.676-11 (annex 1, §2.2) to propagate the signal for one layer to the next, starting on Svalsat. The process is repeated for various elevation angles until the elevation angle allowing to join the beacon receiver and the satellite is eventually found within an acceptable error margin. The specific attenuation is then integrated (iii) along the newly found geometric path to recover the total attenuation (dB) at the current time step. This way, 2 years of simulated attenuation time series ($\Delta t =$ 5 min) concurrent with the beacon measurements are generated.

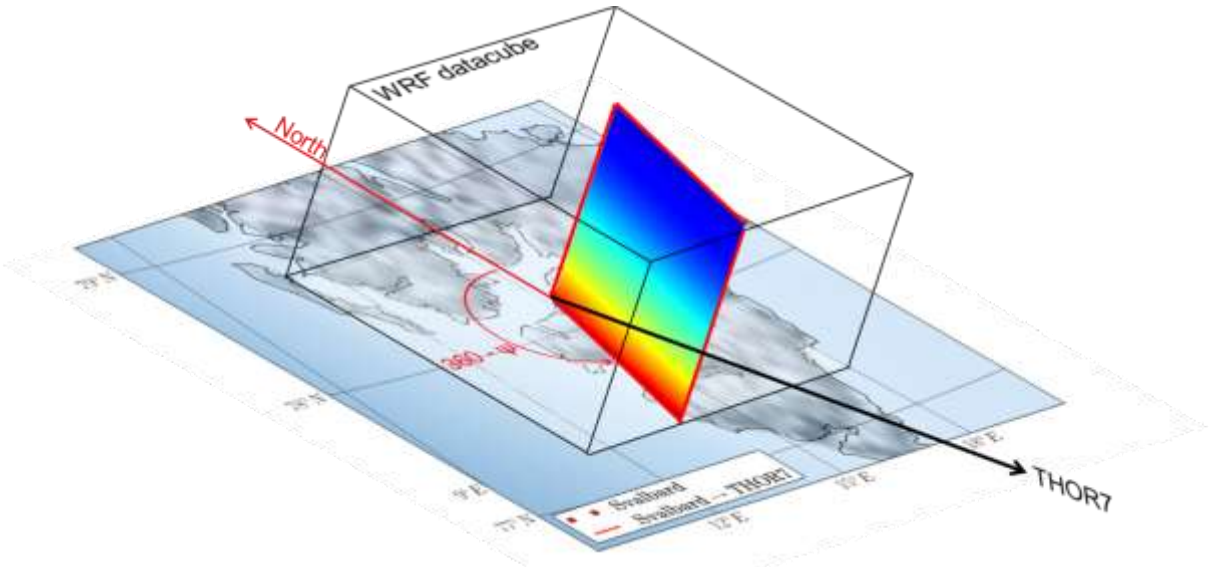

Figure 7 – Vertical slice of atmosphere in the direction of THOR7 @ azimuth ψ (illustration)

5 Results and conclusion

Comparisons between simulated and measured parameters have been conducted both for meteorological surface parameters and tropospheric attenuation.

For year 1 and year 2 of the experiment, measured and simulated surface pressure and temperature at Svalsat and are in very good agreement (see time series example in Figure 8).

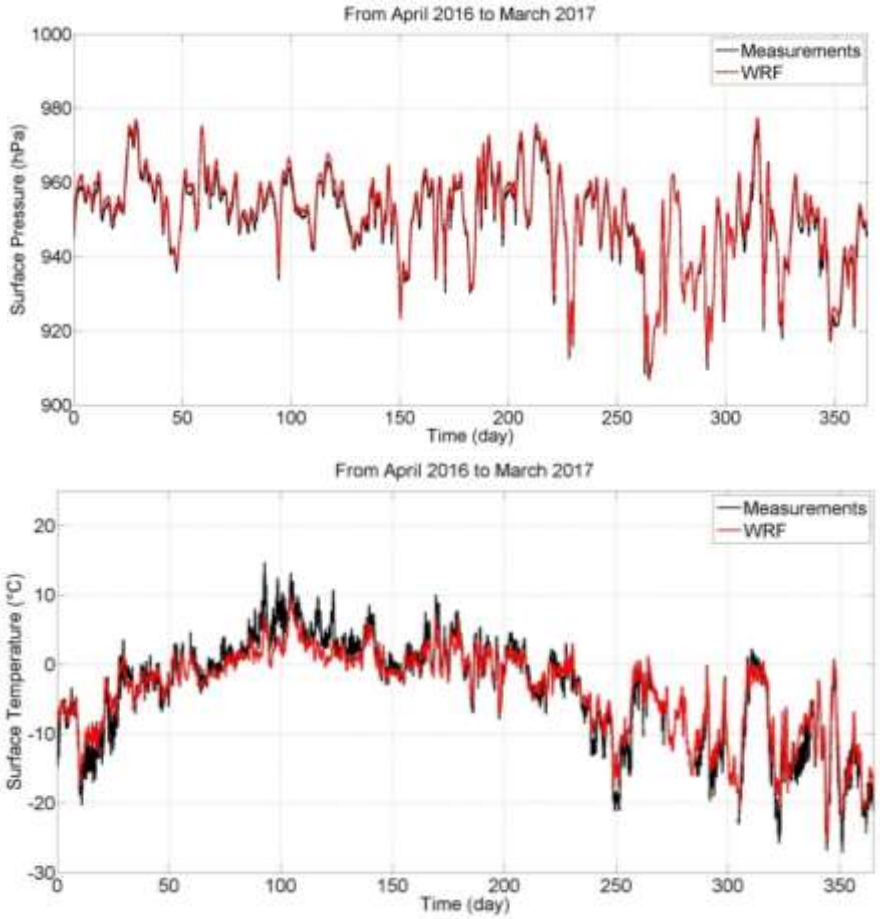

Figure 8 – Surface pressure (up) and temperature (bottom) measured by the meteorological station at Svalsat (black) and generated by the atmospheric model (red).

The total attenuation time series (measured, scintillation not removed, and simulated) show a fairly good agreement (see example for 2 months in Figure 9)

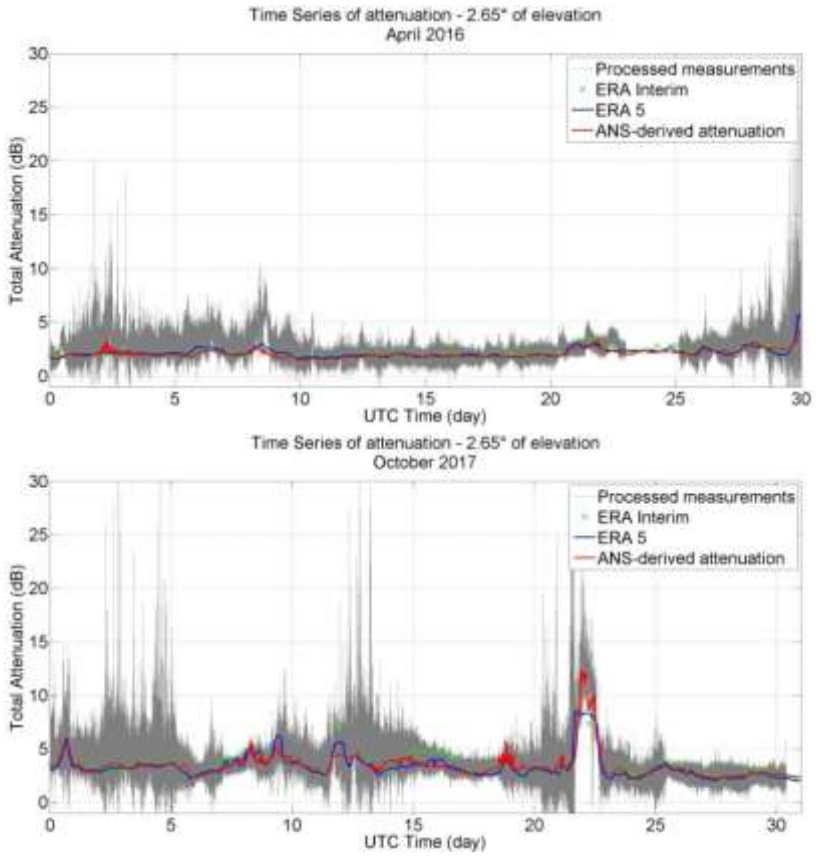

Figure 9 – Total attenuation time series measured by the beacon receiver (grey curve, scintillation not removed), derived from ERA-Interim data every 6h (green cross), derived from ERA5 data every hour (blue curve) and computed from the simulated atmosphere generated by WRF-ARW (red curve)

Finally, the CCDFs of simulated total attenuation have been computed for both years and the comparison with the measured CCDFs is shown in Figure 10.

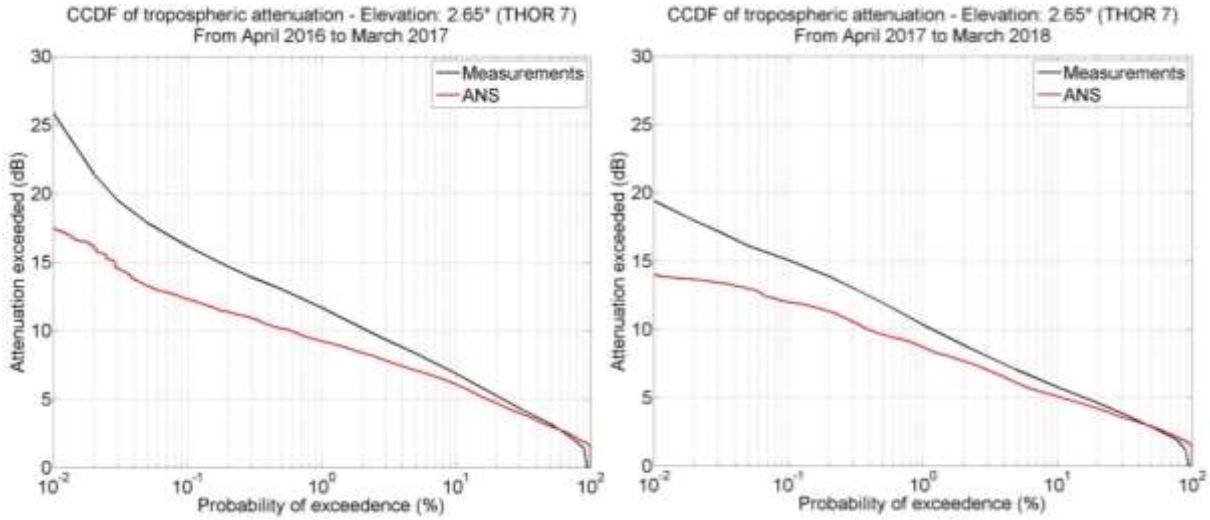

Figure 10 - Total attenuation CCDF measured (black) and simulated (red) for both years

The results for the two years in Figure 10 show a clear underestimation of the attenuation exceeded by the Atmospheric Numerical Simulator, for nearly all percentages of time (≤ 60-70%). The effect of snow –not considered within the simulations generated by the ANS – is probably the main reason of the under prediction of the simulated CCDF with respect to the measured one. Looking at the CCDFs

of solid and liquid precipitations in the left panel of Figure 3, it is clear that snow should be a significant contributor to precipitation rates, and wet snow should be therefore a strong contributor to total attenuation at these frequencies [17]. Moreover, the removal of scintillation by filtering the measured attenuation with a fixed cutt-off frequency could also be responsible for an overestimation of the CCDFs' exceeded attenuation, as it may fail to remove all scintillation from the data.

In order to improve the ANS simulations, various efforts are being made: (i) a snow attenuation physical model is currently developed to be integrated into the electromagnetic module, and (ii) the use of a more resolved database from the ECMWF (*eg.* ERA5: 0.25°x0.25°, every hour) as an input to WRF-ARW is also being investigated.

6 References

[1] F. Carassa, 'The Sirio programme and its propagation and communication experiment', *Alta Freq.*, vol. 47, pp. 65E-71E, Apr. 1978.

[2] T. Ishida, N. Fugono, J. Tabata, M. Ohara, and T. Ishizawa, 'Propagation experiment with Japanese satellite, ETS-II (KIKU-2)', *Acta Astronaut.*, vol. 7, pp. 357–370, 1980.

[3] R. K. Crane, Xuhe Wang, D. B. Westenhaver, and W. J. Vogel, 'ACTS propagation experiment: experiment design, calibration, and data preparation and archival', *Proc. IEEE*, vol. 85, no. 6, pp. 863–878, Jun. 1997.

[4] J. Allnutt, 'INTELSAT propagation experiments: the focus and results of recent campaigns', *Proc. IEEE*, vol. 81, no. 6, pp. 856–864, Jun. 1993.

[5] D. C. Cox and H. W. Arnold, 'Results from the 19- and 28-GHz COMSTAR satellite propagation experiments at Crawford Hill', *Proc. IEEE*, vol. 70, no. 5, pp. 458–488, May 1982.

[6] J. P. V. Poires Baptista and P. G. Davies, 'OPEX Reference Book on Attenuation Measurement and Prediction', Second Workshop of the OLYMPUS Propagation Experimenters, ESTEC Noordwijk, The Netherlands, ESA WPP-083, Nov. 1994.

[7] B. Giannone, E. Saggese, E. Matricciani, and A. Paraboni, 'The Italsat propagation experiment', *Space Commun. Broadcast.*, vol. 3, pp. 221–231, Sep. 1985.

[8] O. Koudelka, 'Q/V-band communications and propagation experiments using ALPHASAT', *Acta Astronaut.*, vol. 69, no. 11, pp. 1029–1037, Dec. 2011.

[9] J. R. Houts, J. A. Nessel, and M. J. Zemba, 'Design of a Ka-band propagation terminal for atmospheric measurements in polar regions', in *2016 10th European Conference on Antennas and Propagation (EuCAP)*, 2016, pp. 1–3.

[10] M. J. Zemba, J. R. Morse, and J. A. Nessel, 'Frequency estimator performance for a software-based beacon receiver', in *2014 IEEE Antennas and Propagation Society International Symposium (APSURSI)*, 2014, pp. 1574–1575.

[11] J. Nessel, M. Zemba, and J. Morse, 'Results from three years of Ka-band propagation characterization at Svalbard, Norway', in *2015 9th European Conference on Antennas and Propagation (EuCAP)*, 2015, pp. 1–5.

[12] M. Rytir, 'Clear-air scintillation and multipath for low-elevation high-latitude satellite communication links', in *2015 9th European Conference on Antennas and Propagation (EuCAP)*, 2015, pp. 1–5.

[13] M. O. García, N. Jeannin, L. Féral, and L. Castanet, 'Use of WRF model to characterize propagation effects in the troposphere', presented at the 2013 7th European Conference on Antennas and Propagation (EuCAP), 2013, pp. 1377–1381.

[14] N. Jeannin *et al.*, 'Atmospheric channel simulator for the simulation of propagation impairments for Ka band data downlink', in *The 8th European Conference on Antennas and Propagation (EuCAP 2014)*, The Hague, Netherlands, 2014, pp. 3357–3361.

[15] W. C. Skamarock *et al.*, 'A Description of the Advanced Research WRF Version 3.', NCAR, Boulder, CO, USA, Tech. Note NCAR/TN-475+STR, 2008.

[16] H. C. Hulst and H. C. van de Hulst, *Light scattering by small particles*. Courier Corporation, 1981.

[17] W. I. Linlor, 'Permittivity and attenuation of wet snow between 4 and 12 GHz', *J. Appl. Phys.*, vol. 51, no. 5, pp. 2811–2816, May 1980.